CrystEngComm

ROYAL SOCIETY OF CHEMISTRY

COMMUNICATION

View Article Online
View Journal | View Issue

Cite this: *CrystEngComm*, 2025, **27**, 7638

Received 9th September 2025,
Accepted 23rd October 2025

DOI: 10.1039/d5ce00870k

rsc.li/crystengcomm

Halopyridinium cations as bifunctional donors of halogen and hydrogen bonds in salts with benzenesulfonic and *p*-toluenesulfonic acids†

Matija Čulig,[ab] Vinko Nemec, *[a] Nikola Bregović [a] and Dominik Cinčić *[a]

A selection of 10 mono- and dihalopyridines have been used as salt coformers for benzenesulfonic and *p*-toluenesulfonic acids. In most cases, the resultant halopyridinium cations are bifunctional donors of both charge-assisted hydrogen and halogen bonds to the sulfonate anions.

Strong intermolecular interactions like hydrogen (HBs) and halogen bonds (XBs) determine how molecular building units will connect in the crystal.[1–4] Understanding these interactions enables the rational design of crystalline materials, single-component as well as multi component solids, with tailored structures and properties.[4–9] Due to their directionality and predictability, HBs and XBs are among the most studied intermolecular interactions, with applications in the crystal engineering of both organic and metal–organic systems.[1,4,10–14] Their strengths range from weak (~10 kJ mol^{-1}) to strong (>40 kJ mol^{-1}).[15,16] Halogen bonds, characterised by a localised σ-hole, are generally more directional than hydrogen bonds and can be finely tuned by varying the halogen atom or adjacent substituents.[17–21] Despite extensive studies on systems dominated by either HB or XB, the interplay between them—especially in cocrystals of neutral bifunctional HB/XB donors—remains relatively underexplored.[22,23] The Cambridge Structural Database (CSD)[24] contains only 65 entries on multicomponent systems involving nitrogen-based acceptors and simple HB/XB bifunctional donors *e.g.* perhalogenated anilines, phenols, benzoic acids, and *N*-(benzylidene)hydroxylamines, representing the majority of studied systems featuring neutral HB/XB bifunctional donors.[25–30] However, another well-established approach to studying systems containing bifunctional HB/XB donors involves salts based on halogenated aromatic amines and halogenated *N*-heterocycles (*e.g.* halopyridines).[31–38] Over the past two decades, both protonated and *N*-alkylated halogenopyridines have been extensively investigated as halogen bond donors, forming interactions with a variety of organic and inorganic anions.[10,39–49] Similar to neutral halogen bond donors, the strength of cationic halogen bond donors decreases from iodo- to chloro-substituted derivatives.[32,36,49] Stilinović and co-workers have recently performed a structural and computational study of the potential of halopyridinium cations as halogen bond donors.[36] They investigated iodide salts of mono-halogenated pyridine derivatives in both protonated and *N*-methylated forms and have shown that although protonation and *N*-methylation of halogenopyridines enhance the electrostatic potential (ESP) of the halogen σ-hole, this site is not always the most positive region on the cation, especially in chloropyridinium derivatives. In these cases, hydrogen and carbon atoms often exhibit higher ESP values, explaining the low frequency of halogen bonding in their crystal structures. In accord with their findings and considerations, our analysis of the CSD on crystal structures containing simple 2-, 3- and 4-halopyridinium cations has shown two general trends, firstly, that iodopyridinium cations reliably form halogen bonds regardless of the position (about 80% frequency for 2-halopyridinium cations and over 90% for 4-halopyridinium cations), while bromopyridinium and chloropyridinium cations have similar frequencies for each position of the halogen atom, and secondly, that 2- and especially 4-halopyridinium cations are significantly more frequent halogen bond donors (Table S4).[24] The larger halogen size may compensate for lower ESP, facilitating stronger halogen bonding through reduced steric hindrance and increased contact surface. Thus, while halopyridinium cations are not necessarily superior to neutral donors, iodopyridinium species in particular serve

[a] *Department of Chemistry, Faculty of Science, University of Zagreb, Horvatovac 102a, 10000 Zagreb, Croatia. E-mail: vnemec@chem.pmf.hr, dominik@chem.pmf.hr*
[b] *R&D Pliva Croatia Ltd., member of Teva group, Prilaz baruna Filipovića 25, 10000 Zagreb, Croatia*

† Dedicated to Professor Resnati, celebrating a career in fluorine and noncovalent chemistry on the occasion of his 70th birthday.

as reliable bifunctional HB/XB donors and are valuable tools in the design of halogen- and hydrogen-bonded supramolecular architectures.

As a step towards further exploration of both the potential and the limitations of halogenopyridinium cations as bifunctional HB/XB donors with larger organic anions, in this research, we selected a series of mono- and dihalopyridines: 3-chloropyridine (**3Clpy**), 3-bromopyridine (**3Brpy**), 3-iodopyridine (**3Ipy**), 4-iodopyridine (**4Ipy**), 2,6-dichloropyridine (**26diClpy**), 2,6-dibromopyridine (**26diBrpy**), 3,5-dichloropyridine (**35diClpy**), 3,5-dibromopyridine (**35diBrpy**), 5-bromo-2-chloropyridine (**5Br2Clpy**) and 5-bromo-2-iodopyridine (**5Br2Ipy**) (Scheme 1) and combined them with two highly acidic sulfonic acids, benzenesulfonic (**bsaH**, pK_a = −2.7) and *p*-toluenesulfonic acids (**ptsaH**, pK_a = −5.4).[50] Our hypothesis was that the combination of sulfonic acids with halopyridines would result in the protonation of the pyridyl nitrogen atom, allowing us to obtain salts featuring strong N–H···O hydrogen bonds. Since these acids can be multitopic acceptors of hydrogen or halogen bonds through their three oxygen atoms, we expected the simultaneous presence of X···O halogen bonding, which would depend on the halopyridine used. Specifically, we anticipated that bromo- and iodopyridines would form halogen bonds, while chloropyridines would not, in accordance with previous studies.[36,51,52] Additionally, we were interested in evaluating the effect of the position of halogen atoms both in mono- and dihalopyridines on the overall cation–anion network.

Salt screening experiments were performed by liquid-assisted grinding (LAG) and crystallisation from solutions. Bulk products of the **5Br2Ipy** salts required for further characterisation were also obtained by slurrying reactant mixtures for several days in *n*-hexane. Mechanochemical experiments were performed on a Retsch MM200 Shaker Mill using stainless steel jars and stainless steel balls under normal laboratory conditions (temperature *ca.* 25 °C, 40–60% relative humidity, see the SI for details). Crystallisation experiments were performed by dissolving a reactant mixture in an appropriate solvent, with heating, followed by letting the solvent or solvent mixture cool down and evaporate at room temperature. The obtained products were characterised by powder (PXRD) and single-crystal X-ray diffraction (SCXRD), as well as by differential scanning calorimetry (DSC). Potentiometric and UV/vis spectrophotometric titrations of mono- and dihalopyridines with dilute hydrochloric acid or perchloric acid were performed in order to determine the pK_a values of pyridines and to compare their Lewis basicities with the results obtained in the solid state (see the SI for titration details, experimental and calculated curves, species distribution curves and UV/vis spectra).

Out of 20 combinations, we obtained a total of 10 novel solids by crystallisation experiments from a solution of reactants, which were all characterised by SCXRD and found out to be salts. Of those, eight were obtained by LAG (Table 1). Milling **3Clpy** and **ptsaH**, **3Brpy** and **ptsaH**, or **35diBrpy** and **ptsaH** under the same conditions resulted in liquid products. Slurry experiments were used to obtain bulk amounts of pure (**bsa**)(**5Br2IpyH**) and (**ptsa**)(**5Br2IpyH**) products.

5Br2Ipy was found to be the only dihalopyridine which formed salts when reacted with both acids. The solids obtained by LAG from the systems containing 2,6- or 3,5-dihalopyridine and **bsaH** and **ptsaH** were revealed to be either solid mixtures of the reactants or a mixture of an unknown phase and one of the reactants. Products obtained by milling **35diClpy** and **bsaH**, or **35diBrpy** and **bsaH** could not be fully characterised since solution experiments resulted in mixtures or amorphous phases. In order to rationalise the results of our salt screening, we investigated the protonation properties of the studied pyridine derivatives in aqueous solutions. It is important to emphasise that the aqueous pK_a values have been commonly used to interpret the reactivity of solids in the solid state that potentially involve proton transfer or to rationalise the outcomes of salt or cocrystal screening either mechanochemically or *via* solution crystallisation from a variety of non-aqueous solvents.[53–55] Therefore, the measured pK_a values should be interpreted as a measure of the relative intrinsic basicity of the studied

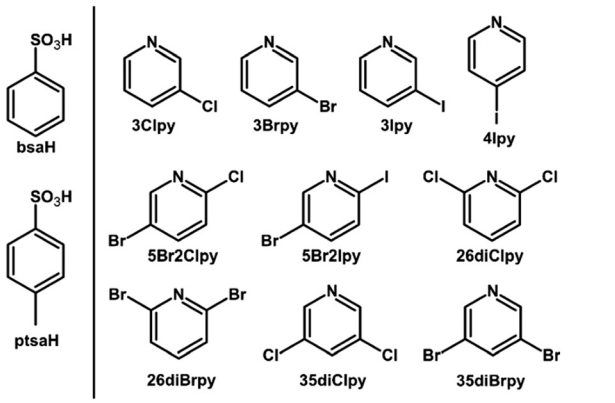

Scheme 1 Molecular structures of sulfonic acids and mono- and dihalopyridines used in this study.

Table 1 Comparison of results obtained mechanochemically (LAG) and by crystallisation experiments in solution (SOL)

	bsaH		ptsaH	
Halopyridine	LAG	SOL	LAG	SOL
3Clpy	+	+	−	+
3Brpy	+	+	−	+
3Ipy	+	+	+	+
4Ipy	+	+	+	+
35diClpy	+	−	−	−
35diBrpy	+	−	−	−
26diClpy	−	−	−	−
26diBrpy	−	−	−	−
5Br2Clpy	−	−	−	−
5Br2Ipy	+	+	+	+

Table 2 Experimentally determined pK_a values for mono- and dihalopyridines used in this study. Both potentiometric and spectrophotometric determinations were performed in water, at an ionic strength of 0.1 mol dm^{-3} and at 25 °C

Halopyridine	pK_a
3Clpy	3.02(1)[a]
3Brpy	3.17(1);[a] 2.91(1)[b]
3Ipy	3.55(1)[a]
4Ipy	4.04(1)[a]
35diClpy	0.37(1)[b]
35diBrpy	0.75(1)[b]

[a] Potentiometric value. [b] Spectrophotometric value.

pyridine derivatives and should not be correlated with proton transfer mechanisms under the used LAG conditions (where the liquid phase has a catalytic role, can influence the molecular diffusion, the crystallinity of the product, *etc.*)[56–58] and crystallisation conditions.[55] We performed pH potentiometric titrations (see the SI for experimental details) which enabled the determination of pK_a values for **3Clpy**, **3Brpy**, **3Ipy**, and **4Ipy** (Table 2). On the other hand, the presence of **26diClpy**, **26diBrpy**, **35diClpy**, **35diBrpy** or **5Br2Clpy** in the titrated solution had no evident effect on the pH which suggested that these compounds featured rather low basicity. Therefore, we performed spectrophotometric titrations, which is a method suitable for the determination of such low pK_a values given that the characteristic spectra of the protonation species differ significantly. Indeed, as excess of acid was added to the solutions of investigated pyridines, significant spectral changes were detected and the obtained titration curves could be processed by assuming protonation of the pyridine molecule. This approach enabled quantitative characterisation of protonation properties for **35diClpy** and **35diBrpy** and yielded pK_a values lower than 1, confirming that the basicity of these compounds is rather low (Table 2). Furthermore, when **26diClpy** and **26diBrpy** were titrated with perchloric acid, no spectral changes occurred, even after more than 5000 molar equivalents of acid were added. This strongly suggested that the protonation of the 2,6-substitued derivatives is an extremely unfavorable process.

A comparison of the results obtained by the two methods for **3Brpy** shows that they give similar values; therefore, the spectrophotometric values can be used in conjunction with potentiometric ones for the purpose of establishing a trend. It should be mentioned that the pK_a value for **5Br2Ipy** could not be determined, because of too low solubility of the compound. The results described above provide a strong foundation for the rationalisation of the fact that salts of 2,6- and 3,5-dihalopyridines could not be obtained. Namely, our results strongly indicate that these pyridines simply feature too low a basicity for proton transfer from the studied organic acids to be thermodynamically favorable in any medium, including in the solid state. Surprisingly, it seems that the basicity is so low that not even hydrogen bonded cocrystals could be formed.

Structural analysis of the obtained salts revealed that the expected charge-assisted N–H···O hydrogen bonds are formed in all ten cases. Additionally, X···O halogen bonds (X = I, Br, Cl) are present in the structure of the salts with bromo- and iodo-substitued pyridines and in (**3ClpyH**)(**bsa**). On the other hand, Cl···O halogen bonds have been found in (**3ClpyH**)(**ptsa**), a trend that is in line with previous studies affirming the chlorine atom as the weakest halogen bond donor. Hydrogen bonds N–H···O and all halogen bonds and their corresponding parameters are listed in Table 3. A characteristic typical for the 3-chloropyridinium and 3-bromopyridinium salts is the formation of a tetrameric cation–anion structural motif. In (**3ClpyH**)(**ptsa**), the tetramer is formed by a combination of N–H···O and C–H···O hydrogen bonds (Fig. 1a), and tetramers are then connected into a 3D network by a combination of C–H···Cl, C–H···π and additional C–H···O contacts. The tetramer motif in (**3ClpyH**)(**bsa**), (**3BrpyH**)(**bsa**) and (**3BrpyH**)(**ptsa**) is formed by a combination of N–H···O and Br···O or Cl···O bonding (Fig. 1b–d). In these **bsa** salts, one oxygen atom is a simultaneous hydrogen and halogen bond acceptor, while in the **ptsa** salt the tetramer is established through two

Table 3 Geometric parameters of N–H···O hydrogen and halogen bonds in the obtained salts

Salt	d(N–H···O)/Å	Angle/°	X···A	d(X···A)/Å	Angle/°	R.S.[a]/%
(**3ClpyH**)(**bsa**)	2.776	171.3	Cl1···O1	3.308	152.8	0.3
(**3ClpyH**)(**ptsa**)	2.750	172.6	—	—	—	—
(**3BrpyH**)(**bsa**)	2.918	167.9	Br1···O3	3.136	158.5	6.6
(**3BrpyH**)(**ptsa**)	2.598	163.9	Br1···O2	3.284	163.6	2.3
(**3IpyH**)(**bsa**)	2.699	159.9	I1···O3	2.973	173.1	16.0
(**3IpyH**)(**ptsa**)	2.629	162.5	I1···O3	3.253	164.7	8.1
	—	—	I1···O2	3.464	163.5	2.1
(**4IpyH**)(**bsa**)	2.684	171.6	I1···O3	2.998	171.4	15.3
(**4IpyH**)(**ptsa**)	2.670	175.3	I1···O2	2.951	173.9	16.6
(**5Br2IpyH**)(**bsa**)	2.662	175.5	I1···O3	2.835	171.8	19.9
	2.871	157.3	I2···O2	3.059	171.7	13.6
	—	—	Br2···O2	3.074	153.7	8.5
(**5Br2IpyH**)(**ptsa**)	2.709	176.9	I1···O1	2.798	170.8	21.0

[a] R.S. = 1 – d(D···A)/[r_{vdW}(D) + r_{vdW}(A)]; r_{vdW} are Alvarez's van der Waals radii.[59]

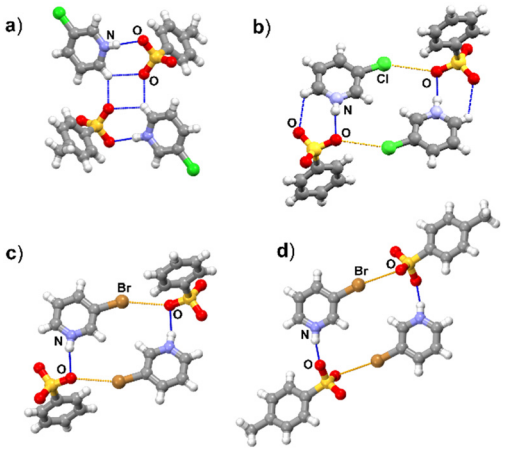

Fig. 1 Halogen and hydrogen bonded tetramers in crystal structures of: a) (**3ClpyH**)(**ptsa**), b) (**3ClpyH**)(**bsa**), c) (**3BrpyH**)(**bsa**) and d) (**3BrpyH**)(**ptsa**).

different oxygen atoms. In (**3ClpyH**)(**bsa**) and (**3BrpyH**)(**bsa**), these tetramers are further connected first into a chain by bifurcated C–H···O hydrogen bonds and then into a 3D network by a combination of additional C–H···O and C–H···π hydrogen bonds, while in (**3BrpyH**)(**ptsa**) these tetrameric units connect into a 3D network by additional C–H···O hydrogen bonds. The tetramer motif is also present in (**3IpyH**)(**ptsa**), where it is formed by a combination of N–H···O and I···O bonding, and where the iodine atom is a bifurcated donor (Fig. 2b). The connectivity yielding the 3D network is achieved through a combination of C–H···O and C–H···I hydrogen bonds and stacking. In (**3IpyH**)(**bsa**), N–H···O and I···O halogen bonds lead to the formation of an undulating chain that is further stabilised by C–H···O hydrogen bonds (Fig. 2a). The chains are connected into a 3D network through additional C–H···O hydrogen bonds. As we hypothesised, a change in the position of the iodine substituent on the pyridine ring leads to a significantly different network.

In (**4IpyH**)(**bsa**), chains in the crystal structure are formed by I···O halogen bonds in cooperation with N–H···O and C–H···O hydrogen bonds that form a $R_2^2(7)$ motif. Two parallel chains are then connected into a wider chain by additional C–H···O hydrogen bonds; these resultant chains are connected into layers by C–H···π contacts, and the layers are then stacked in the 3D structure. On the other hand, in (**4IpyH**)(**ptsa**), chains are formed by a combination of N–H···O hydrogen and I···O halogen bonds (Fig. 2c and d), and the **ptsa** anions alternate between two orientations. The chains in (**4IpyH**)(**ptsa**) are further connected into 2D layers by C–H···O hydrogen bonds. As already stated, only two salts including dihalopyridines have been obtained, both involving **5Br2IpyH**. The main similarity between the structures of (**5Br2IpyH**)(**ptsa**) and (**5Br2IpyH**)(**bsa**) lies in the fact that a combination of I···O and strong N–H···O bonds leads to the formation of a zipper-like chain (Fig. 3a). In the **ptsa** salt, the chains are then connected into a 3D network by numerous C–H···O hydrogen bonds. In (**5Br2IpyH**)(**bsa**), two symmetrically inequivalent **bsa** and **5Br2IpyH** ions are present. While one ion pair forms the aforementioned chain, the other cation and anion are statistically disordered (see the SI for details), also forming a chain held together by N–H···O and C–H···O hydrogen bonds.

This chain is linked to nearby zipper-like chains *via* I···O and Br···O halogen bonds (Fig. 3b). The final 3D network is obtained by combining all of the mentioned interactions with additional C–H···O hydrogen bonds.

Thermal analysis results show that in most cases there is a single, well-defined peak corresponding to the melting point in the temperature range of 111–157 °C (Table 4). Three trends can be identified: 1) salt melting or decomposition temperatures are well above the melting temperatures of both the sulfonic acid and the used halopyridine; 2) salts with **bsa** have higher melting or decomposition temperatures than corresponding **ptsa** salts, an exception being **5Br2IpyH** salts, where the opposite is the case; 3) exchanging a halogen atom for another that is a stronger halogen bond donor results in a slight increase in the melting or decomposition temperature (the only exception is (**3ClpyH**)(**bsa**)).

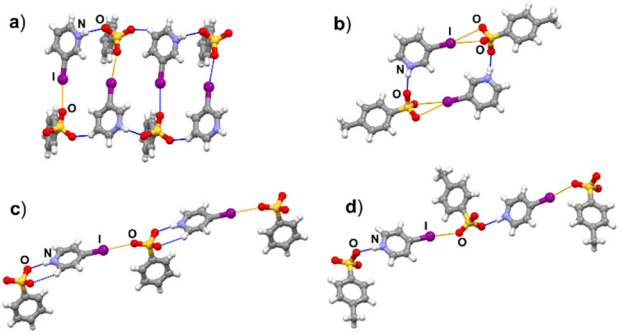

Fig. 2 Parts of supramolecular chains in crystal structures of: a) (**3IpyH**)(**bsa**), b) (**3IpyH**)(**ptsa**), c) (**4IpyH**)(**bsa**), and d) (**4IpyH**)(**ptsa**).

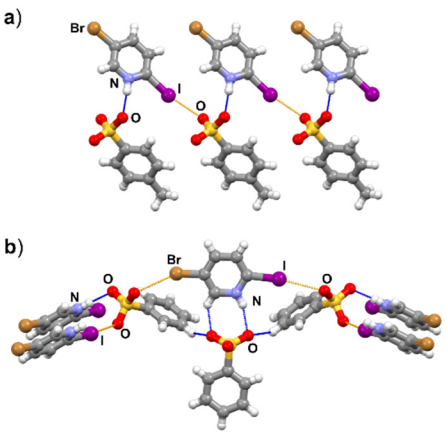

Fig. 3 Parts of supramolecular chains in crystal structures of: a) (**5Br2IpyH**)(**ptsa**) and b) (**5Br2IpyH**)(**bsa**). Disordered formula units in b) are omitted for clarity.

Table 4 Onset temperatures (t_e) of melting and decomposition processes in salt DSC curves, and tabulated values for sulfonic acids and halopyridines that are solids at 25 °C

Compound	t_e/°C
(**3ClpyH**)(**bsa**)	138
(**3ClpyH**)(**ptsa**)	111
(**3BrpyH**)(**bsa**)	130
(**3BrpyH**)(**ptsa**)	110
(**3IpyH**)(**bsa**)	135
(**3IpyH**)(**ptsa**)	125
(**4IpyH**)(**bsa**)	136[a]
(**4IpyH**)(**ptsa**)	115[a]
(**5Br2IpyH**)(**bsa**)	138
(**5Br2IpyH**)(**ptsa**)	156
bsaH	51[b]
ptsaH	38[b]
3Ipy	53–56[b]
4Ipy	80[b]
5Br2Ipy	112–113[b]

[a] Decomposition temperature. [b] Tabulated value.

Conclusions

To conclude, we have successfully synthesised ten salts of benzenesulfonic and *p*-toluenesulfonic acids with a series of mono- and dihalopyridines. In accord with previous findings and our hypothesis, the obtained structural data allow us to ascertain that the dominant intermolecular interactions in these systems are charge-assisted hydrogen bonds formed upon proton transfer from the acid to the pyridine nitrogen atom. The next most important interactions are the X···O halogen bonds, of which I···O are expectedly stronger (according to the geometric parameters) than Br···O and Cl···O halogen bonds. Monohalopyridines have been determined to be more reliable as hydrogen bond donors. According to our results, this is due to their higher basicity compared to dihalopyridines, combined with the observed lack of Cl···O halogen bonding and relative weakness of Br···O halogen bonding. Therefore, bromo- and iodopyridines have been confirmed as potential bifunctional donor molecules in systems involving strong organic acids. With regards to **bsaH** and **ptsaH**, both acids have proven amenable coformers for halopyridines of high enough basicity, as the resulting **bsa** and **ptsa** ions were shown to be polytopic hydrogen and halogen bond acceptors that could participate in the formation of a variety of supramolecular architectures.

Author contributions

Investigation: MČ performed the synthesis of salts and the crystallisation experiments. Conceptualisation: VN, NB and DC conceived and designed the study and formulated research aims. Formal analysis: VN performed single-crystal X-ray diffraction measurements, thermal analysis and the associated data processing. MČ and NB performed the determination of pK_a values. Supervision: the study was supervised by VN and DC. Visualisation: VN and DC prepared the schemes and figures. Writing: the manuscript draft was written by VN with contributions from all authors. Reviews and editing were done by VN and DC. DC ensured funding acquisition and project management.

Conflicts of interest

There are no conflicts to declare.

Data availability

The data supporting this article (experimental procedures, DSC curves, PXRD patterns, crystal data and ORTEP representations of obtained structures, potentiometric and spectrophotometric data) have been included as part of the supplementary information (SI). Supplementary information is available. See DOI: https://doi.org/10.1039/d5ce00870k.

CCDC 2484628–2484637 contain the supplementary crystallographic data for this paper.[60a–j]

Acknowledgements

This research was funded by the Croatian Science Foundation under the research project IP-2019-04-1868. Additionally, we acknowledge support of the project CIuK cofinanced through the European Regional Development Fund-Competitiveness and Cohesion Operational Programme (Grant KK.01.1.1.02.0016). The authors are very grateful to Marina Ratkaj for helping with SCXRD data collection.

Notes and references

1 G. R. Desiraju, *J. Am. Chem. Soc.*, 2013, **135**, 9952–9967.
2 G. R. Desiraju, *Angew. Chem., Int. Ed.*, 2007, **46**, 8342–8356.
3 C. B. Aakeröy, S. V. Panikkattu, B. DeHaven and J. Desper, *Cryst. Growth Des.*, 2012, **12**, 2579–2587.
4 G. Cavallo, P. Metrangolo, R. Milani, T. Pilati, A. Priimagi, G. Resnati and G. Terraneo, *Chem. Rev.*, 2016, **116**, 2478–2601.
5 K. M. Hutchins, *R. Soc. Open Sci.*, 2018, **5**, 180564.
6 J.-C. Christopherson, F. Topić, C. J. Barrett and T. Friščić, *Cryst. Growth Des.*, 2018, **18**, 1245–1259.
7 K. T. Mahmudov, M. N. Kopylovich, M. F. C. Guedes da Silva and A. J. L. Pombeiro, *Coord. Chem. Rev.*, 2017, **345**, 54–72.
8 A. Mukherjee, S. Tothadi and G. R. Desiraju, *Acc. Chem. Res.*, 2014, **47**, 2514–2524.
9 D. Yan, D.-K. Bučar, A. Delori, B. Patel, G. O. Lloyd, W. Jones and X. Duan, *Chem. – Eur. J.*, 2013, **19**, 8213–8219.
10 R. Bertani, P. Sgarbossa, A. Venzo, F. Lelj, M. Amati, G. Resnati, T. Pilati, P. Metrangolo and G. Terraneo, *Coord. Chem. Rev.*, 2010, **254**, 677–695.
11 T. Steiner, *Angew. Chem., Int. Ed.*, 2002, **41**, 48–76.
12 V. Nemec, K. Lisac, N. Bedeković, L. Fotović, V. Stilinović and D. Cinčić, *CrystEngComm*, 2021, **23**, 3063–3083.
13 M. K. Corpinot and D.-K. Bučar, *Cryst. Growth Des.*, 2019, **19**, 1426–1453.

14 A. Mukherjee, S. Tothadi and G. R. Desiraju, *Acc. Chem. Res.*, 2014, **47**, 2514–2524.
15 K. Wendler, J. Thar, S. Zahn and B. Kirchner, *J. Phys. Chem. A*, 2010, **114**, 9529–9536.
16 P. J. Costa, *Phys. Sci. Rev.*, 2017, **2**, 20170136.
17 V. Stilinović, G. Horvat, T. Hrenar, V. Nemec and D. Cinčić, *Chem. – Eur. J.*, 2017, **23**, 5244–5257.
18 D. Cinčić, T. Friščić and W. Jones, *Chem. – Eur. J.*, 2008, **14**, 747–753.
19 M. Kolář, J. Hostaš and P. Hobza, *Phys. Chem. Chem. Phys.*, 2014, **16**, 9987–9996.
20 C. Präsang, A. C. Whitwood and D. W. Bruce, *Cryst. Growth Des.*, 2009, **9**, 5319–5326.
21 P. Metrangolo, F. Meyer, T. Pilati, G. Resnati and G. Terraneo, *Angew. Chem., Int. Ed.*, 2008, **47**, 6114–6127.
22 C. C. Robertson, J. S. Wright, E. J. Carrington, R. N. Perutz, C. A. Hunter and L. Brammer, *Chem. Sci.*, 2017, **8**, 5392–5398.
23 C. B. Aakeröy, P. D. Chopade and J. Desper, *Cryst. Growth Des.*, 2011, **11**, 5333–5336.
24 C. R. Groom, I. J. Bruno, M. P. Lightfoot and S. C. Ward, *Acta Crystallogr., Sect. B: Struct. Sci., Cryst. Eng. Mater.*, 2016, **72**, 171–179.
25 C. B. Aakeröy, M. Fasulo, N. Schultheiss, J. Desper and C. Moore, *J. Am. Chem. Soc.*, 2007, **129**, 13772–13773.
26 C. B. Aakeröy, S. Panikkattu, P. Chopade and J. Desper, *CrystEngComm*, 2013, **15**, 3125–3136.
27 C. B. Aakeröy, N. Schultheiss, A. Rajbanshi, J. Desper and C. Moore, *Cryst. Growth Des.*, 2009, **9**, 432–441.
28 M. D. Perera, J. Desper, A. S. Sinha and C. B. Aakeröy, *CrystEngComm*, 2016, **18**, 8631–8636.
29 C. B. Aakeröy, C. L. Spartz, S. Dembowski, S. Dwyre and J. Desper, *IUCrJ*, 2015, **2**, 498–510.
30 N. Baus Topić, S. G. Dash, E. Topić, M. Arhangelskis and D. Cinčić, *Cryst. Growth Des.*, 2024, **24**, 5078–5088.
31 M. Oszajca, L. Smrčok, H. Pálková and W. Łasocha, *J. Mol. Struct.*, 2012, **1021**, 70–75.
32 K. Raatikainen, M. Cametti and K. Rissanen, *Beilstein J. Org. Chem.*, 2010, **6**, 1.
33 R. J. Attrell, C. M. Widdifield, I. Korobkov and D. L. Bryce, *Cryst. Growth Des.*, 2012, **12**, 1641–1653.
34 K. Kubo, K. Takahashi, S. Nakagawa, K. I. Sakai, S. I. Noro, T. Akutagawa and T. Nakamura, *Cryst. Growth Des.*, 2021, **21**, 2340–2347.
35 L. Fotović and V. Stilinović, *CrystEngComm*, 2020, **22**, 4039–4046.
36 L. Fotović, N. Bedeković and V. Stilinović, *Cryst. Growth Des.*, 2021, **21**, 6889–6901.
37 F. Zordan, S. L. Purver, H. Adams and L. Brammer, *CrystEngComm*, 2005, **7**, 350–354.
38 N. Jakupec, L. Fotović and V. Stilinović, *CrystEngComm*, 2020, **22**, 8142–8150.
39 L. H. Thomas, M. S. Adam, A. O'Neill and C. C. Wilson, *Acta Crystallogr., Sect. C: Cryst. Struct. Commun.*, 2013, **69**, 1279–1288.
40 F. F. Awwadi, R. D. Willett, K. A. Peterson and B. Twamley, *J. Phys. Chem. A*, 2007, **111**, 2319–2328.
41 M. Freytag, P. G. Jones, B. Ahrens and A. K. Fischer, *New J. Chem.*, 1999, **23**, 1137–1139.
42 G. Mínguez Espallargas, F. Zordan, L. Arroyo Marin, H. Adams, K. Shankland, J. van de Streek and L. Brammer, *Chem. – Eur. J.*, 2009, **15**, 7554–7568.
43 L. Brammer, G. Mínguez Espallargas and H. Adams, *CrystEngComm*, 2003, **5**, 343–345.
44 G. Mínguez Espallargas, L. Brammer and P. Sherwood, *Angew. Chem., Int. Ed.*, 2006, **45**, 435–440.
45 S. Derossi, L. Brammer, C. A. Hunter and M. D. Ward, *Inorg. Chem.*, 2009, **48**, 1666–1677.
46 L. Fotović and V. Stilinović, *Crystals*, 2021, **11**, 1240.
47 J. E. Ormond Prout, P. Smart and L. Brammer, *Cryst. Growth Des.*, 2012, **12**, 205–216.
48 V. Amendola, G. Bergamaschi, M. Boiocchi, N. Fusco, M. V. La Rocca, L. Linati, E. Lo Presti, M. Mella, P. Metrangolo and A. Miljkovic, *RSC Adv.*, 2016, **6**, 67540–67549.
49 L. Fotović, N. Bedeković and V. Stilinović, *Cryst. Growth Des.*, 2022, **22**, 1333–1344.
50 J. P. Guthrie, *Can. J. Chem.*, 1978, **56**, 2342–2354.
51 L. Fotović, N. Bedeković, K. Pičuljan and V. Stilinović, *Cryst. Growth Des.*, 2022, **22**, 7508–7517.
52 L. Posavec, V. Nemec, V. Stilinović and D. Cinčić, *Cryst. Growth Des.*, 2021, **21**, 6044–6050.
53 A. J. Cruz-Cabeza, *CrystEngComm*, 2012, **14**, 6362–6365.
54 V. Stilinović and B. Kaitner, *Cryst. Growth Des.*, 2012, **12**, 5763–5772.
55 S. L. Childs, G. P. Stahly and A. Park, *Mol. Pharmaceutics*, 2007, **4**, 323–338.
56 D. Braga, S. L. Giaffreda, K. Rubini, F. Grepioni, M. R. Chierotti and R. Gobetto, *CrystEngComm*, 2007, **9**, 39–45.
57 T. Friščić, S. L. Childs, S. A. A. Rizvi and W. Jones, *CrystEngComm*, 2009, **11**, 418–426.
58 T. Friščić and W. Jones, *Cryst. Growth Des.*, 2009, **9**, 1621–1637.
59 S. Álvarez, *Dalton Trans.*, 2013, **42**, 8617–8636.
60 (*a*) CCDC 2484628: Experimental Crystal Structure Determination, 2025, DOI: 10.5517/ccdc.csd.cc2pdg9w; (*b*) CCDC 2484629: Experimental Crystal Structure Determination, 2025, DOI: 10.5517/ccdc.csd.cc2pdgbx; (*c*) CCDC 2484630: Experimental Crystal Structure Determination, 2025, DOI: 10.5517/ccdc.csd.cc2pdgcy; (*d*) CCDC 2484631: Experimental Crystal Structure Determination, 2025, DOI: 10.5517/ccdc.csd.cc2pdgdz; (*e*) CCDC 2484632: Experimental Crystal Structure Determination, 2025, DOI: 10.5517/ccdc.csd.cc2pdgf0; (*f*) CCDC 2484633: Experimental Crystal Structure Determination, 2025, DOI: 10.5517/ccdc.csd.cc2pdgg1; (*g*) CCDC 2484634: Experimental Crystal Structure Determination, 2025, DOI: 10.5517/ccdc.csd.cc2pdgh2; (*h*) CCDC 2484635: Experimental Crystal Structure Determination, 2025, DOI: 10.5517/ccdc.csd.cc2pdgj3; (*i*) CCDC 2484636: Experimental Crystal Structure Determination, 2025, DOI: 10.5517/ccdc.csd.cc2pdgk4; (*j*) CCDC 2484637: Experimental Crystal Structure Determination, 2025, DOI: 10.5517/ccdc.csd.cc2pdgl5.